C. R. Mecanique 342 (2014) 174–188

Contents lists available at ScienceDirect

Comptes Rendus Mecanique

www.sciencedirect.com

Micromechanics of granular materials – A tribute to Ching S. Chang

Some micromechanical aspects of failure in granular materials based on second-order work

François Nicot [a,*], Nejib Hadda [a], Luc Sibille [b], Farhang Radjai [c], Pierre-Yves Hicher [d], Félix Darve [e]

[a] Irstea, domaine universitaire, 2, rue de la Papeterie, 38400 Saint-Martin-d'Hères cedex, France
[b] Institut de recherche en génie civil et mécanique, Université de Nantes, ECN-CNRS, Nantes, France
[c] Laboratoire de mécanique et de génie civil, Université de Montpellier, Montpellier, France
[d] Institut de recherche en génie civil et mécanique, École centrale de Nantes, Nantes, France
[e] UJF-INPG-CNRS, Laboratoire Sols Solides Structures Risques, Grenoble, France

ARTICLE INFO

Article history:
Available online 20 February 2014

Keywords:
Stress
Large deformations
Second-order work
Granular materials
Homogenization
Multiscale
Micromechanics
Microstructure

ABSTRACT

This paper discusses the notion of failure in a granular assembly by examining the key microstructural mechanisms which are most likely to trigger the nucleation and propagation of instabilities within a granular material. For this purpose, the key variable to predict the occurrence of failure, known as second-order work, is expressed from variables on the grain scale. The local behaviour incidents (where contacts may open or slide), compared to the global response of the assembly, are analysed by two approaches. First, numerical computations made by a discrete element model confirm the microscopic definition of the second-order work. Secondly, a micromechanical model, based on a homogenization procedure, relating the macroscopic behaviour to microscopic ingredients, namely contact planes, points to a close link between the occurrence of failure on the macroscopic scale as well as on the contact planes.

1. Introduction

It is of vital importance to geotechnical practice to understand the modes of failure in granular materials. The practical question is how a granular system such as a foundation or a talus in a state of mechanical equilibrium can continue to withstand the external loads acting at the boundary and in the bulk of a system in response to a perturbation in the loading conditions or in the system characteristics, e.g., weakening of a material strength parameter. The perturbations may have different origins, such as seismic loading or accumulation of grains by sedimentation, which can act as extra loads on the structure, and various environmental disturbances with a weathering effect on the material, such as grain damage by weathering or contact lubrication, loss of grains by erosion leading to a looser state of the grain assembly. In general, both types of perturbation may be treated in a common framework by normalizing the external loads with the appropriate strength parameters of the system.

The system is stable if small stress increments $\delta\sigma_{ij}$ are accommodated by small deformations $\delta\varepsilon_{ij}$ at every point of the system, so that the new equilibrium state is close to the undisturbed state. The grain-scale process underlying this transition between two consecutive equilibrium states is generally stochastic due to disorder and unilateral contacts between grains,

* Corresponding author.
E-mail address: francois.nicot@irstea.fr (F. Nicot).

http://dx.doi.org/10.1016/j.crme.2014.01.006
1631-0721/

but if the stress and strain variations have a finite average value, a tangent *constitutive tensor* $D_{ijkl} = \delta\sigma_{ij}/\delta\varepsilon_{kl}$ can be defined from their ratio in the macroscopic limit. Hence, the existence and uniqueness of this tensor defines tautologically a *quasistatic path* as opposed to a dynamic (unstable) evolution, irrespective of the nature of deformations.

In a conservative system (elastic deformations only), the stresses derive from a potential function ψ ($\sigma_{ij} = \mathrm{d}\psi/\mathrm{d}\varepsilon_{ij}$) so that a stable equilibrium state, corresponding to a local minimum of ψ, is characterized by the positive definiteness of the constitutive tensor, i.e. $D_{ijkl}\delta\varepsilon_{ij}\delta\varepsilon_{kl} > 0$. This is no more and no less than the expression of the *second-order work* $W_2 = D_{ijkl}\delta\varepsilon_{kl}\delta\varepsilon_{ij} = \delta\sigma_{ij}\delta\varepsilon_{ij}$, whose positivity was first shown by Hill to be a sufficient condition for stability, including the case of irreversible deformations [1]. In this generalization from conservative to dissipative materials, failure may occur only if the second-order work vanishes or becomes negative along a loading path.

It is essential to note that the second-order criterion by itself does not provide a sufficient condition for failure. But when W_2 vanishes along a loading path, the material may become unstable with a *bifurcation* from a quasistatic regime towards a dynamic regime. By definition, the second-order work vanishes at the plastic threshold, but it may also vanish below the plastic threshold in granular materials as a result of the asymmetry of the constitutive tensor, reflecting the fact that the direction of shear strain is independent of the yield surface (given by the internal angle of friction). As a consequence, the potential energy stored in the granular configuration by dilation may in principal transform spontaneously to shear deformation so that the material may keep deforming without further energy input. In contrast to localized structures appearing prior to failure in the form of shear zones or compaction bands at the plastic threshold, the failure appearing in the bifurcation domain below the plastic threshold is homogeneous or *diffuse*, in close analogy with liquefaction where the instability fully spreads to the bulk as a consequence of load transfer from the contact network to the pore liquid [2].

In a granular material, the stresses and strains are functions of the contact force and grain displacements, respectively. Hence, the second-order work and failure criteria, very briefly sketched above, may be based on the granular micromechanics. In this respect and quite fundamentally, a grain-scale expression of the second-order work becomes a powerful concept that may be applied in order to investigate physical origins of failure, the influence of material parameters, as well as the nucleation and propagation of instabilities inside a granular material. This is a challenging issue regarding the unilateral contact interactions allowing for rearrangements of the contact network and the dynamic heterogeneities induced by excluded-volume effects [3,4].

In this paper, we present a micromechanical approach with the aim of identifying the relevant microscopic variables contributing to the second-order work in a representative volume element, on the one hand, and to illustrate its applicability both in discrete-element simulations and in models inspired by granular micromechanics. The theoretical background is first introduced in Section 2 with a particular accent put on the link between the second-order work and the increase of kinetic energy. A microscopic expression of the second-order work is then derived in Section 3 from very general considerations and compared to numerical data obtained by discrete-element simulations in Section 4. Finally, a micromechanical model is presented in Section 5 as an example of the development of instability when an explicit expression of the constitutive tensor is given. The most salient results of this work will be summarized and discussed in Section 6.

2. Theoretical background

What is failure in a material? How can this concept be defined, prior to any analytical investigation? The different answers to these basic questions are perhaps the reason why we witness a diversity of approaches to describe failure in geomechanics. The leading idea proposed in a series of papers [5,6] is that when failure occurs for a given material, a class of perturbations takes place which cause an increase in the kinetic energy of a body. If we assume that the body was in a state of equilibrium just before failure, then we witness a transition from a static regime toward a dynamical regime associated with inertial mechanisms. For this reason, the equilibrium state is reputed to be unstable. Therefore, when failure occurs within a material, it is reasonable to analyse how the kinetic energy of the system may evolve. For this purpose, the following equation plays a central role by relating the increase in kinetic energy $E_c(t+\delta t) - E_c(t)$ to the competition between internal mechanisms involving the constitutive behaviour of the material (W_2), and the boundary loading (B_2) involving only the external domain [7]:

$$E_c(t+\delta t) - E_c(t) = \frac{1}{2}(B_2 - W_2) \tag{1}$$

The term B_2 is computed from the displacements and forces acting on the boundary of the system, whereas the term W_2 corresponds to the second-order work that is expressed through a Lagrangian formalism as [1]:

$$W_2 = \int_{V_0} \delta\Pi_{ij}\delta F_{ij}\,\mathrm{d}V_0 \tag{2}$$

where V_0 is the volume of the system, $\overline{\overline{\Pi}}$ denotes the Piola–Kirchoff stress tensor of the first type, and F_{ij} is the general term of the displacement gradient tensor. The second-order work is therefore associated with the incremental evolution $(\delta\Pi_{ij}, \delta F_{ij})$, where both incremental quantities δF_{ij} and $\delta\Pi_{ij}$ are related through the constitutive equation.

On the basis of assuming small deformations and of disregarding geometrical aspects [7,8], the literature has commonly admitted that the second-order work can be expressed in Eulerian conditions as:

$$W_2 = \int_{V_0} \delta\sigma_{ij}\delta\varepsilon_{ij}\,\mathrm{d}V_0 \tag{3}$$

where $\bar{\bar{\sigma}}$ denotes the Cauchy stress tensor, and $\bar{\bar{\varepsilon}}$ is the strain tensor in small deformation conditions. Both incremental quantities $\delta\varepsilon_{ij}$ and $\delta\sigma_{ij}$ are related through the (Eulerian) constitutive equation.

Basically, according to Eq. (1), the kinetic energy of the system can adopt strictly positive values if $W_2 < B_2$. It can be shown that this situation is likely to appear along various loading paths as soon as a generalized limit state is reached [6]. In such a case, $W_2 = 0$ and the kinetic energy will increase, if B_2 is negative.

The expression (3) has been considered by many authors who checked whether the second-order work can vanish and take negative values. It was shown, by considering different constitutive models [9–11], different discrete element methods [12,13], or experimental approaches [14,15], that the second-order work can vanish well before the plastic limit is reached. As highlighted in Eq. (2), the definition of the second-order work intrinsically involves the constitutive behaviour of the system, so that the vanishing of the second-order work depends upon specific material properties, such as the initial porosity.

For materials and loading history experiencing a vanishing of the second-order work, it has been shown that the second-order work has negative values along specific (stress or strain) loading directions contained within a cone [9,10,16–18]. These directions specify which loading controls could be inclined to lead the system to failure.

A major challenge that remains is to understand the underpinning micromechanical mechanisms that govern the vanishing of the second-order work. To continue work along this line, it is worthwhile to construct a link between the microscopic (involving the particle scale) and the macroscopic (involving the specimen, or the system scale) domains. This is the purpose of the next section, where a basic relationship is inferred between the macroscopic second-order work (Eq. (2)) and a dual term (microscopic second-order work) computed from local variables.

3. An attempt to bridge both micro and macro worlds

The second-order work, as defined in Eq. (2) or in Eq. (3), is a macroscopic term related to a system or a material point. In the specific case of granular materials, it would be of interest to express the second-order work with microscopic variables, taking into account the microstructure of the material. To this purpose, a granular assembly composed of N grains 'p', with $1 \leqslant p \leqslant N$, is being considered. No specific restriction is imposed upon the shape of the grains. The mass of each grain 'p' is denoted m_p. At a given time t, each grain 'p' is in contact with n_p other grains 'q' = 'p_k', with $k = 1, \ldots, n_p$, and the total number of contacts at this time t within the assembly is denoted N_c. Boundary particles, belonging to the boundary ∂V, are distinguished from the internal particles belonging to the inner volume $\widehat{V} = V - \partial V$ strictly inside the boundary.

The system is assumed to be in equilibrium at a given time t under a prescribed external loading. Depending on the type of loading control, each grain 'p' belonging to the boundary ∂V of the volume is subjected to a displacement (kinematic control) or to an external force $\bar{f}^{\mathrm{ext},p}$ (static control), possibly nil on given parts of ∂V.

The Eulerian Love–Weber formula expresses the macroscopic stress tensor within a specimen of volume V, in equilibrium under the external forces $\bar{f}^{\mathrm{ext},p}$ applied to the boundary particles 'p' of position $\bar{x}^p$ [8,19–22]:

$$\sigma_{ij} = \frac{1}{V}\sum_{c=1}^{N_c} f_i^c l_j^c + \frac{1}{V}\sum_{p\in V} f_i^p x_j^p \tag{4}$$

where $\bar{l}^c$ is the branch vector relating the centres of contacting particles, $\bar{f}^p$ denotes the resultant force applied to the particle 'p', and $\bar{f}^c$ is the contact force existing between adjoining particles.

When the micro inertial effects are negligible, or when all particles are in equilibrium, the second term, $\frac{1}{V}\sum_{p\in V} f_i^p x_j^p$, can be omitted. When internal dynamic effects exist with local unbalance, this term should be taken into account.

In the Eulerian formulation given in Eq. (4), the contact forces, the branch vectors, the location of each particle, and the volume of the specimen are likely to evolve over a given loading history from an initial configuration $C_0(\bar{f}_0^c, \bar{l}_0^c, \bar{x}_0^c, V_0)$. Referring to this initial configuration, the Lagrangian stress tensor reads:

$$\Pi_{ij} = \frac{1}{V_0}\sum_{p,q} f_i^c l_{0,j}^c + \frac{1}{V_0}\sum_{p\in V_0} f_i^p x_{0,j}^p \tag{5}$$

The tensor $\bar{\bar{\Pi}}$, as a Lagrangian stress tensor, is computed from the current forces with respect to the fixed, initial configuration. Thus, the differentiation of Eq. (5) reads:

$$\delta\Pi_{ij} = \frac{1}{V_0}\sum_{p,q} \delta f_i^c l_{0,j}^c + \frac{1}{V_0}\sum_{p\in V_0} \delta f_i^p x_{0,j}^p \tag{6}$$

By considering that at time t both initial and current configurations coincide (updated Lagrangian configuration), $\bar{l}^c = \bar{l}_0^c$, $\bar{x}^p = \bar{x}_0^p$, $\bar{\bar{F}} = \bar{\bar{I}}$, $V = V_0$ and $J = 1$, and Eq. (6) can be expressed as:

$$\delta \Pi_{ij} = \frac{1}{V} \sum_{p,q} \delta f_i^c l_j^c + \frac{1}{V} \sum_{p \in V} \delta f_i^p x_j^p \tag{7}$$

Thus, as $W_2 = V \delta \Pi_{ij} \delta F_{ij}$, the following relation holds:

$$W_2 = \sum_{p,q} \delta f_i^c \delta l_i^c + \sum_{p \in V} \delta f_i^p \delta x_i^p + \frac{1}{2} \sum_{p,q} f_i^c \left(\delta^2 l_i^c - \delta^2 F_{ij} l_j^c \right) + \frac{1}{2} \sum_{p \in V} \delta f_i^p \left(\delta^2 x_i^p - \delta^2 F_{ij} x_j^p \right) \tag{8}$$

This expression can be transformed by replacing the summation over all the contacts with a summation over the particles. By doing so, we obtain:

$$\sum_{p,q} f_i^c \delta^2 l_i^c = \frac{1}{2} \sum_{p=1}^{N} \sum_{q=1}^{N} f_i^{p,q} \delta^2 l_i^{q,p} \tag{9}$$

where $\bar{f}^{p,q}$ denotes the force applied by the particle 'p' onto the particle 'q', and $\bar{l}^{q,p}$ the vector branch from the particle 'q' to the particle 'p'. When no contact exists between particles 'p' and 'q', then $\bar{f}^{p,q}$ is nil.

Then, taking into account that $l_i^{q,p} = x_i^p - x_i^q$ and $f_i^{p,q} = -f_i^{q,p}$, Eq. (9) can be expressed as:

$$\sum_{p,q} f_i^c \delta^2 l_i^c = -\sum_{p \in V} \left(\left(\sum_{q \in V} f_i^{q,p} \right) \delta^2 x_i^p \right) \tag{10}$$

Given an internal particle 'p', $\sum_{q \in V} \bar{f}^{q,p}$ represents the resultant force $\bar{f}^p$ applied by the adjoining particles to the particle 'p'. For a boundary particle 'p', $\bar{f}^p = \sum_{q \in V} \bar{f}^{q,p} + \bar{f}^{\text{ext},p}$. Thus, Eq. (10) becomes:

$$\sum_{p,q} f_i^c \delta^2 l_i^c = -\sum_{p \in V} f_i^p \delta^2 x_i^p + \sum_{p \in \partial V} f_i^{\text{ext},p} \delta^2 x_i^p \tag{11}$$

Similarly,

$$\sum_{p,q} f_i^c \delta^2 F_{ij} l_j^c = -\sum_{p \in V} f_i^p \delta^2 F_{ij} x_j^p + \sum_{p \in \partial V} f_i^{\text{ext},p} \delta^2 F_{ij} x_j^p \tag{12}$$

It follows that:

$$\sum_{p,q} f_i^c \left(\delta^2 l_i^c - \delta^2 F_{ij} l_j^c \right) + \sum_{p \in V} f_i^p \left(\delta^2 x_i^p - \delta^2 F_{ij} x_j^p \right) = \sum_{p \in \partial V} f_i^{\text{ext},p} \left(\delta^2 x_i^p - \delta^2 F_{ij} x_j^p \right) \tag{13}$$

Eq. (8) reads therefore:

$$W_2 = \sum_{p,q} \delta f_i^c \delta l_i^c + \sum_{p \in V} \delta f_i^p \delta x_i^p + \frac{1}{2} \sum_{p \in \partial V} f_i^{\text{ext},p} \left(\delta^2 x_i^p - \delta^2 F_{ij} x_j^p \right) \tag{14}$$

Assuming that the loading directs macro-homogeneous strain and stress fields within the specimen in the spirit of Hill [23], the incremental displacement $\delta \bar{u}$ of a material point of position $\bar{X}$ belonging to the boundary ∂V of the volume is a homogeneous function of degree one with respect to the position $\bar{X}$, so that:

$$\delta u_i = \delta x_i = \frac{\partial (\delta u_i)}{\partial X_j} X_j = \delta F_{ij} X_j \quad \text{and} \quad \delta^2 u_i = \delta^2 x_i = \delta^2 F_{ij} X_j \tag{15}$$

When both initial and current configurations coincide, $\bar{X} = \bar{x}$, and:

$$\delta x_i = \delta F_{ij} x_j \quad \text{and} \quad \delta^2 x_i = \delta^2 F_{ij} x_j \tag{16}$$

Thus, Eq. (14) simplifies into:

$$W_2 = \sum_{p,q} \delta f_i^c \delta l_i^c + \sum_{p \in V} \delta f_i^p \delta x_i^p \tag{17}$$

Eq. (17) shows that the micromechanical expression of the second-order work is the combination of two terms. The first term $W_2^m = \sum_{p,q} w_2^c$, with $w_2^c = \delta f_i^c \delta l_i^c$ can be related to the local second-order work $\sum_{p,q} \delta f_i^c \delta u_i^c$ [7], and embeds the intricate link between both the contact force network and the geometrical distribution of branches between grains.

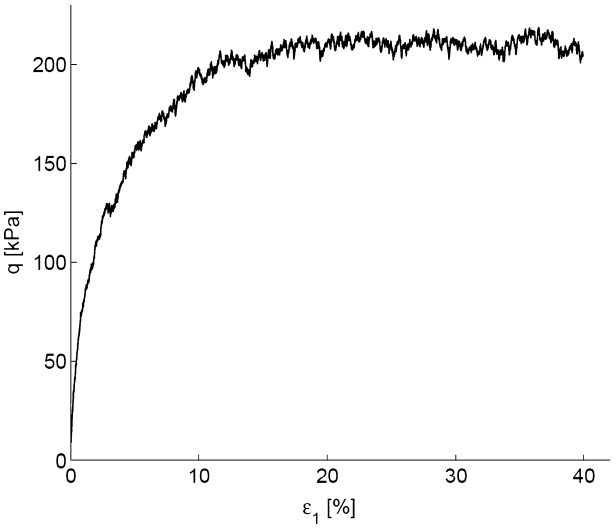

Fig. 1. Deviatoric stress in terms of the axial strain at 200 kPa of confining pressure.

The second term $\sum_{p\in V}\delta f_i^p \delta x_i^p$ of Eq. (17) introduces the incremental unbalanced force $\delta \bar{f}^p$ applied to each particle 'p'. When inertial effects are negligible, the contribution of this term becomes negligible as well. But when particles become highly rearranged inside the plastic regime (sliding between particles, contact opening and contact creation), this term is likely to be no longer negligible.

Finally, Eq. (17) constitutes the micromechanical expression of the second-order work, giving rise to possible microstructural investigation of the vanishing of the second-order work; basically a necessary condition for failure to occur [5,6,16].

4. Numerical investigation from a discrete element method

The analytic development detailed in the previous section, shows that the macroscopic second-order work can be expressed in terms of two microstructural quantities $\sum_{p,q}\delta f_i^c \delta l_i^c$ and $\sum_{p\in V}\delta f_i^p \delta x_i^p$ (Eq. (17)) depending on both the contact forces and the geometrical positions of the particles in a grain assembly.

On the basis of this analytical result, it would be interesting to examine numerically how far the microscopic second-order work, as defined in Eq. (17), can match the macroscopic second-order work by using the discrete element method.

In this section, we will turn our attention toward the numerical validation of the balance between the left- and right-hand terms of Eq. (17).

4.1. Numerical model

Numerical simulations were conducted using software 'Yade' [24] based on the discrete element method [25] and with a three-dimensional loosely compacted assembly of particles (porosity is around 0.43).

In the normal direction to the tangential contact plane, the contact constitutive relation is linear elastic and the force is by assumption linearly related to the particle overlap through the constant stiffness. In the tangential direction, the constitutive relation is linear elastic–perfectly plastic. The normal and tangential contact stiffness values are denoted by k_n and k_t, respectively. The friction is incorporated at the contact level by the Coulomb friction law $|f_t^c| \leqslant \mu |f_n^c|$, where f_n^c and f_t^c are the normal and tangential components of the force at contact c, respectively. When this threshold is reached, the tangential relative motion is regarded as sliding with a friction force $\mu|f_n^c|$ directed opposite to the tangential relative velocity. Moreover, only compressive normal forces are allowed, since for tensile normal forces, the contact is considered to split open for cohesionless materials.

The considered specimen has a cubical shape and is composed of 10,000 spherical particles with radii ranging from 2 to 18 mm, enclosed within six rigid frictionless walls.

The parameters in the contact constitutive relation are selected such that $k_n/D_s = 356$ (MPa) and $k_t/k_n = 0.42$, where D_s is the mean diameter of the two particles in contact. The interparticle friction coefficient μ is set to 0.7. A damping coefficient $\lambda^a = 0.05$ for Cundall's non-viscous damping [26] was used in all discrete element simulations.

The assembly was compacted from an initially sparse arrangement of particles to an isotropic state by increasing particle sizes until the isotropic pressure $\sigma_3 = 200$ kPa is reached. It was then subjected to an axisymmetric drained triaxial compression. The evolution of both the deviatoric stress $q = \sigma_1 - \sigma_3$ and the volume variation $\Delta V/V$ versus the axial strain ε_1 are shown in Figs. 1 and 2, respectively.

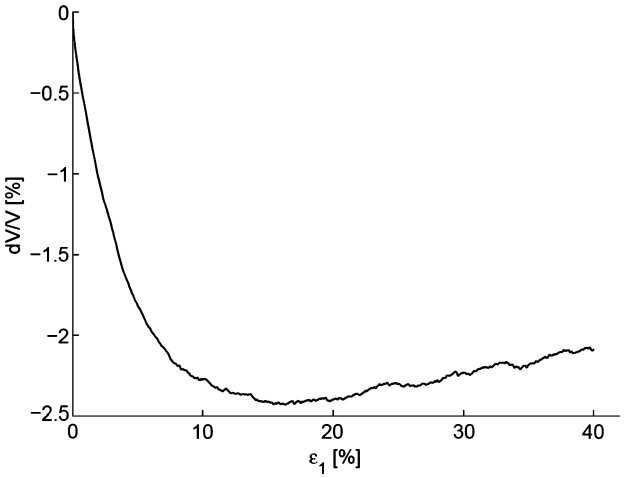

Fig. 2. Volume variation in terms of the axial strain at 200 kPa of confining pressure.

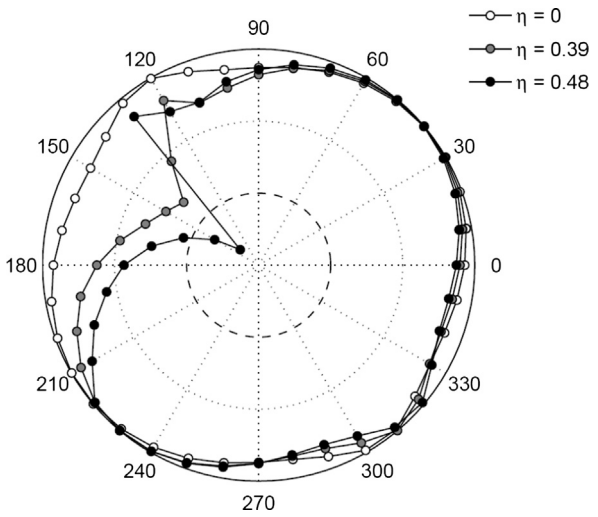

Fig. 3. Circular diagrams of the second-order work in the Rendulic strain increment plane.

As expected for loose materials, the deviatoric stress increases continuously (positive hardening regime) toward a limit plateau at which $q \sim 200$ kPa, and a mainly contractant volumetric behaviour is observed.

4.2. Computation of second-order work from macroscopic variables

In this section, the second-order work is computed from macroscopic variables and for different strain loading directions. For this objective, strain probes (as first introduced by Gudehus [27]) were performed in the Rendulic plane of strain increments (i.e. the axisymmetric plane of strain increments). Strain probes consist of a series of strain loading increments $\Delta\bar{\varepsilon}$, all applied to the granular assembly from the same initial stress–strain state arbitrarily chosen. The strain loading increments fall on a circle of radius $\|\Delta\bar{\varepsilon}\|$ in the Rendulic strain plane. Therefore, each strain loading increment is defined by its direction α_ε (varying here from 0° to 360° with a step of 10°) and its norm $\|\Delta\bar{\varepsilon}\|$ (set here equal to 5×10^{-5} and applied over 5×10^3 time steps).

Once the response vector $\Delta\bar{\sigma}$ is computed for each strain loading increment, the macroscopic normalized second-order work can be computed as $W_2 = \Delta\bar{\varepsilon} \cdot \Delta\bar{\sigma} / \|\Delta\bar{\varepsilon}\| \cdot \|\Delta\bar{\sigma}\|$ [28], for all directions α_ε investigated.

Fig. 3 shows examples of circular diagrams of second-order work, plotted from different initial deviatoric stress ratios defined by $\eta = \frac{q}{p}$, where p is the mean pressure in the specimen.

To make these representations easily legible, a constant $K = 0.5$ has been added to the computed value of W_2. Consequently, when W_2 is negative, the plot is inside the dashed circle of radius $r = K$, whereas the plot is outside the dashed circle for positive values of W_2.

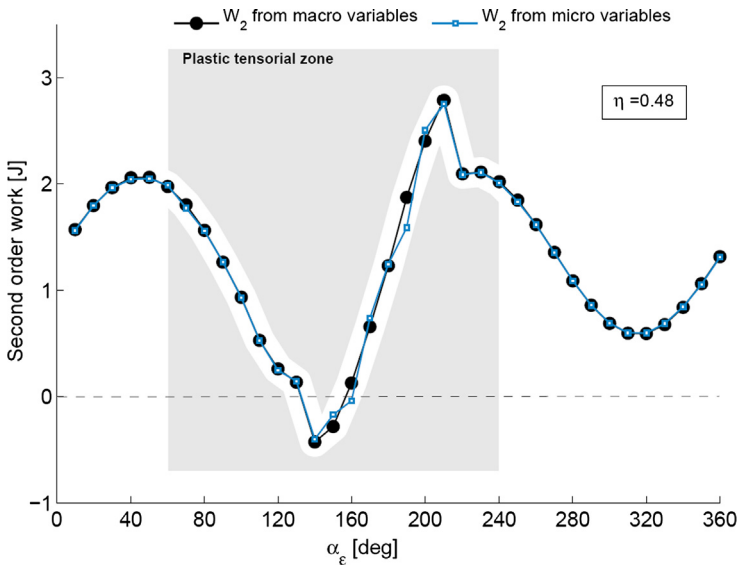

Fig. 4. Comparison between macroscopic and microscopic second-order works.

The cone of instability, gathering the incremental strain directions along which the second-order work takes negative values, is obtained in the second quadrant, defined by $(-\sqrt{2}\Delta\varepsilon_3, \Delta\varepsilon_1)$ of the axisymmetric strain increment plane for the initial deviatoric stress ratio $\eta = 0.48$.

4.3. Computation of second-order work from microscopic variables

The second-order work can also be computed according to Eq. (17) from contact forces ($\bar{f}^c$), position vector of particles ($\bar{x}^p$) and unbalanced forces $\bar{f}^p$ acting on each particle p.

To determine the first scalar product $\delta f_i^c \delta l_i^c$ of Eq. (17), the increment $\delta \bar{f}^c$ is computed as the incremental change of the contact force experienced by the considered contact during a strain probing in direction α_ε. The branch vector increment $\delta \bar{l}^c$ is deduced from the displacement, during the same strain probing, of the particles p and q involved in the contact: $\delta \bar{l}^c = (\delta \bar{x}^p - \delta \bar{x}^q)$. When a contact opens, the scalar product $\delta f_i^c \delta l_i^c$ does not contribute to the summation. In the same way, the second scalar product $\delta f_i^p \delta x_i^p$ is calculated for each particle from increments $\delta \bar{f}^p$ and $\delta \bar{x}^p$ computed over the strain probing in direction α_ε.

Finally, to compute, for a direction α_ε, the value of the second-order work from microscopic variables, scalar products are summed up over all the contacts in the specimen for the first term $\sum_{p,q} \delta f_i^c \delta l_i^c$ and over all particles in the specimen for the second term $\sum_{p \in V} \delta f_i^p \delta x_i^p$.

Fig. 4 shows the change of the second-order work (not normalized) from both macroscopic and microscopic variables at $\eta = 0.48$ in terms of the direction of the strain loading increment α_ε.

The second-order works from both macroscopic and microscopic variables are compared and the two representative curves fit substantially very well.

In the plastic tensorial zone[1] corresponding to $\alpha_\varepsilon \in [60, 240°]$ (the zone in light grey in the figure), fluctuations of second-order work computed from microscopic variables around the macroscopic one can be observed for some directions of strain probes.

In this zone, the inertial effects (taken into account in the computation of the second term $\sum_{p \in V} \delta f_i^p \delta x_i^p$) are supposed to become more significant since the rearrangement of particles intensifies due to the opening and/or the creation of contacts. Since only initial (at the equilibrium state just before applying strain probes) and final (at the equilibrium state immediately after strain probes are applied) stress strain states are used to compute the second-order work, not all openings or creations of contacts experienced during the strain probes can be taken into account, especially when they occur successively (and more than once) for a given pair of particles during a strain probe. This lack of information may result in a non-correspondence between the second-order work from micro- and macro-variables in some directions α_ε in the plastic tensorial zone, as shown in Fig. 4. In the elastic tensorial zone, this fluctuation hardly persists and is negligible.

Based on the analysis above, a discrete element solution is shown to be in good agreement with the micromechanical formalism of the second-order work.

[1] The plastic tensorial zone groups all directions where corresponding total responses to strain increment loading probes have a predominant plastic component compared to the elastic component.

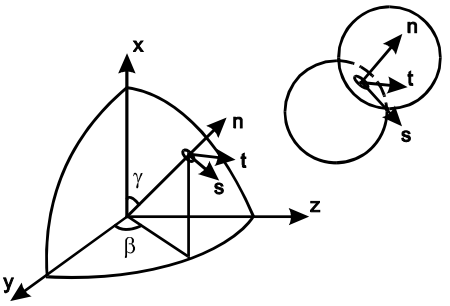

Fig. 5. Local coordinates.

The main conclusion that has to be emphasized is that the macroscopic second-order work can be quite well approximated by the term $\sum_{p,q} \delta f_i^c \delta l_i^c$. Even within the plastic tensorial zone, the contribution of the second term $\sum_{p\in V} \delta f_i^p \delta x_i^p$ (that takes inertial effects into account) remains small with respect to the first term $\sum_{p,q} \delta f_i^c \delta l_i^c$. The term $\sum_{p,q} \delta f_i^c \delta l_i^c$ introduces microstructural variables, hence drawing a bridge between the micro and macro scales. This is particularly convenient when using micromechanical models, as the one considered in the next section, because such models introduce explicitly the microscopic scale (related to the contacts between grains). The micromechanical models can therefore be used to investigate the extent to which and just how the vanishing of the terms $\delta f_i^c \delta l_i^c$, along certain contact direction, may affect the sign of the macroscopic second-order work.

5. Illustration from a micromechanically-based model

Homogenization techniques for granular materials have been developed in the first place to predict their elastic properties [29–34]. More recently, the same techniques have been applied for modelling non-reversible behaviour [35,36]. The basic idea for most of these models is to consider the granular medium as a collection of tangent planes at the contact points between grains, interacting with each other. This approach requires writing the contact law along these tangent planes and developing homogenization operators in order to integrate all these contacts at the scale of the representative elementary volume. Two techniques have been considered. The kinematic approach is based on a localization operator which provides a relationship between intergranular contact displacements and the assembly strain and a homogenization operator which relates the average stress of the granular assembly to a mean field of particle contact forces (see for example [37]). The static approach is based on an inverse technique consisting of a localization operator relating the macro stresses to the local contact forces and a homogenization operator relating the grain displacements to the macro strains. Both approaches relate local forces and displacements through a constitutive law at the contact level. The microstructural model developed by Chang and Hicher [38] is based on a static approach presented in the following section.

5.1. The microstructural model

In this model, a granular material is regarded as a collection of particles. The deformation of a representative volume of the material is generated by mobilizing contact particles in all orientations. Thus, the stress–strain relationship can be derived as an average of the mobilization behaviour of local contact planes in all orientations. For a contact plane in the αth orientation, the local forces f_i^α and the local movements d_i^α can be denoted as follows: $f_i^\alpha = \{f_n^\alpha, f_s^\alpha, f_t^\alpha\}$ and $d_i^\alpha = \{d_n^\alpha, d_s^\alpha, d_t^\alpha\}$, where the subscripts n, s, and t represent the components in the three directions of the local coordinate system. The direction normal to the plane is denoted as n; the other two orthogonal directions, s and t, are tangential to the plane (Fig. 5).

The forces and movements at the contact planes of all orientations are suitably superimposed to obtain the macroscopic stress strain tensors. The macroscopic stiffness tensor is obtained on the condition that the rate of energy dissipation expressed in terms of the macro stress and strain must be equivalent to that expressed in terms of micro forces and movements. Under such a formulation, it has usually been assumed that the microstructure is statically constrained, which means that the forces on each contact plane are assumed to balance the resolved components of the macroscopic stress tensor.

5.1.1. Micro–macro relationship

The stress–strain relationship for an assembly can be determined by integrating the behaviour of interparticle contacts in all orientations. In the integration process, a micro–macro relationship is required. Following the Love–Weber approach (Eq. (4)), and assuming that only small deformations occur (so that both Eulerian and Lagrangian formulations coincide), the incremental stress increment can be obtained by the contact forces and branch vectors for all contacts, as follows:

$$\delta\sigma_{ij} = \frac{1}{V}\sum_{\alpha=1}^{N} \delta f_j^\alpha l_i^\alpha \tag{18}$$

The mean force on the contact plane of each orientation is

$$\delta f_j^{\alpha} = V A_{ik}^{-1} \delta \sigma_{ij} \tag{19}$$

where the fabric tensor is defined as:

$$A_{ik} = \sum_{\alpha=1}^{N} l_i^{\alpha} l_k^{\alpha} \tag{20}$$

Using the principle of energy balance, which states that the work done in a representative volume element is equal to the work done on all inter-cluster planes within the element [39], we obtain the following relation:

$$\sigma_{ij} \delta \varepsilon_{ij} = \frac{1}{V} \sum_{\alpha=1}^{N} f_j^{\alpha} \delta l_i^{\alpha} \tag{21}$$

From Eqs. (19) and (21), we derive the relation between the global strain and interparticle displacement:

$$\delta \varepsilon_{ij} = A_{ik}^{-1} \sum_{\alpha=1}^{N} l_k^{\alpha} \delta l_j^{\alpha} \tag{22}$$

5.1.2. Stress–strain relationship

From the above equations, the following relationship between stress increment and strain increment can be obtained:

$$\delta \varepsilon_{ij} = C_{ijmp} \delta \sigma_{mp} \tag{23}$$

where $C_{ijmp} = A_{ik}^{-1} A_{mn}^{-1} V \sum_{\alpha=1}^{N} (k_{jp}^{ep})^{-1} l_k^{\alpha} l_n^{\alpha}$.

When the contact number N is sufficiently large in an isotropic packing, the summation of the compliance tensor in Eq. (23) and the summation of the fabric tensor in Eq. (21) can be written in integral form, given by

$$C_{ijmp} = A_{ik}^{-1} A_{mn}^{-1} \frac{NV}{2\pi} \int_0^{\pi/2} \int_0^{2\pi} k_{jp}^{ep}(\gamma, \beta)^{-1} l_k(\gamma, \beta) l_n(\gamma, \beta) \sin\gamma \, \mathrm{d}\gamma \, \mathrm{d}\beta \tag{24}$$

and

$$A_{ik} = \frac{N}{2\pi} \int_0^{\pi/2} \int_0^{2\pi} l_i(\gamma, \beta) l_k(\gamma, \beta) \sin\gamma \, \mathrm{d}\gamma \, \mathrm{d}\beta \tag{25}$$

The integration of Eqs. (24) and (25) in a spherical coordinate can be carried out numerically by using Gauss integration points over the surface of the sphere [38].

5.1.3. Inter-particle behaviour

Elastic stiffness: The contact stiffness of a contact plane α includes normal stiffness, k_n^{α}, and shear stiffness, k_t^{α}. The elastic stiffness tensor is defined by:

$$f_i^{\alpha} = k_{ij}^{\alpha e} d_j^{\alpha e} \tag{26}$$

which can be related to the contact normal and shear stiffness k_n and k_t, respectively:

$$k_{ij}^{\alpha e} = k_n^{\alpha} n_i^{\alpha} n_j^{\alpha} + k_t^{\alpha} \left(s_i^{\alpha} s_j^{\alpha} + t_i^{\alpha} t_j^{\alpha} \right) \tag{27}$$

The value of the stiffness for two elastic spheres can be estimated from Hertz–Mindlin's formulation [40]. For sand grains, a revised form was adopted [31], given by:

$$k_n = k_{n0} \left(\frac{f_n}{G_g l^2} \right)^n; \qquad k_t = k_{t0} \left(\frac{f_n}{G_g l^2} \right)^n \tag{28}$$

where G_g is the elastic modulus for the grains, f_n is the contact force in normal direction, l is the branch length between two particles, k_{n0}, k_{t0} and n are material constants.

Plastic yield function: The yield function is assumed to be of the Mohr–Coulomb type, defined in a contact–force space (e.g. f_n, f_s, f_t):

$$F(f_i, \kappa) = T - f_n \kappa \left(\Delta^p \right) = 0 \tag{29}$$

where $\kappa(\Delta^p)$ is a hardening/softening parameter. The shear force f_r and the rate of plastic sliding Δ^p are defined as:

$$\delta f_r = \sqrt{(\delta f_s)^2 + (\delta f_t)^2} \quad \text{and} \quad \Delta^p = \sqrt{\left(\delta d_s^p\right)^2 + \left(\delta d_t^p\right)^2} \tag{30}$$

The hardening function is defined by a hyperbolic curve in κ–Δ^p plane, which involves two material constants: ϕ_p and k_{p0}.

$$\kappa = \frac{k_{p0} \tan\phi_p \Delta^p}{|f_n| \tan\phi_p + k_{p0}\Delta^p} \tag{31}$$

Plastic flow rule: The plastic sliding often occurs along the tangential direction of the contact plane with an upward or downward movement, thus, shear-induced dilation/contraction takes place. The dilatancy effect can be described by:

$$\frac{\delta d_n^p}{\Delta^p} = \left(\tan\phi_0 - \frac{f_r}{f_n}\right) D \tag{32}$$

where D is a dimensionless material constant which controls the dilation amount during shearing. D takes positive values, meaning that dilation occurs when f_r/f_n becomes bigger than $\tan\phi_0$. The material constant ϕ_0 can be considered in most cases equal to the interparticle friction angle ϕ_μ. This equation can be derived by assuming that the dissipation work for a contact plane due to both normal and shear plastic movements ($f_n \delta d_n^p + f_r \Delta^p D$) is equal to the energy loss due to friction ($f_n \tan\phi_0 \Delta^p D$) at the contact. On the yield surface, under a loading condition, the shear plastic flow is determined by a normality rule applied to the yield function. However, the plastic flow in the direction normal to the contact plane is governed by the stress–dilatancy equation in Eq. (32). Thus, the flow rule is non-associated.

Influence of assembly void ratio: The resistance against sliding in a contact plane is dependent on the degree of interlocking by neighbouring particles. The resistance can be related to the packing void ratio by:

$$\tan\phi_p = \left(\frac{e_c}{e}\right)^m \tan\phi_\mu \tag{33}$$

where m is a material constant [41] and e_c corresponds to the critical void ratio for a given state of stress. For dense packing, e_c/e is greater than 1 and, therefore, the apparent interparticle friction angle ϕ_p is greater than the internal friction angle ϕ_μ. When the packing structure dilates, the degree of interlocking and the apparent friction angle is reduced, which results in a strain-softening phenomenon. For loose packing, the apparent friction angle ϕ_p is smaller than the internal friction angle ϕ_μ and increases during the material contraction.

The critical void ratio e_c is a function of the mean stress applied to the overall assembly and can be written as follows:

$$e_c = \Gamma - \lambda \log(p') \quad \text{or} \quad e_c = e_{\text{ref}} - \lambda \log\left(\frac{p'}{p_{\text{ref}}}\right) \tag{34}$$

where Γ and λ are two material constants, p' is the mean stress of the packing, and $(e_{\text{ref}}, p_{\text{ref}})$ is a reference point on the critical state line.

5.1.4. Elasto-plastic relationship

With the elements discussed above, the incremental force-displacement relationship of the interparticle contact can be obtained. Including both elastic and plastic behaviours, this relationship is given by:

$$\delta f_i^\alpha = k_{ij}^{\alpha p} \delta d_j^\alpha \tag{35}$$

and

$$\begin{bmatrix} \delta f_n \\ \delta f_r \end{bmatrix} = \begin{bmatrix} K_{nn} & K_{nr} \\ K_{rn} & K_{rr} \end{bmatrix} \begin{bmatrix} \delta d_n \\ \delta d_r \end{bmatrix} \tag{36}$$

with $\delta d_r = \sqrt{(\delta d_s)^2 + (\delta d_t)^2}$. Detailed expression of the elasto-plastic stiffness tensor can be derived from the yield function and the flow rule (see [18]). We obtain the following expressions for the components of the constitutive matrix $\overline{\overline{K}}$ at the local scale:

$$K_{nn} = \left(k_{n0} + \frac{k_{n0}^2}{B_0}\left(\tan\phi_p - \frac{f_r}{f_n}\right) D \frac{f_r}{f_n}\right)\left(\frac{f_n}{f_{\text{ref}}}\right)^n \tag{37}$$

$$K_{nr} = -k_{n0}\left(\frac{k_{n0}}{B_0}\left(\tan\phi_p - \frac{f_r}{f_n}\right) D k_{rR}\right)\left(\frac{f_n}{f_{\text{ref}}}\right)^n \tag{38}$$

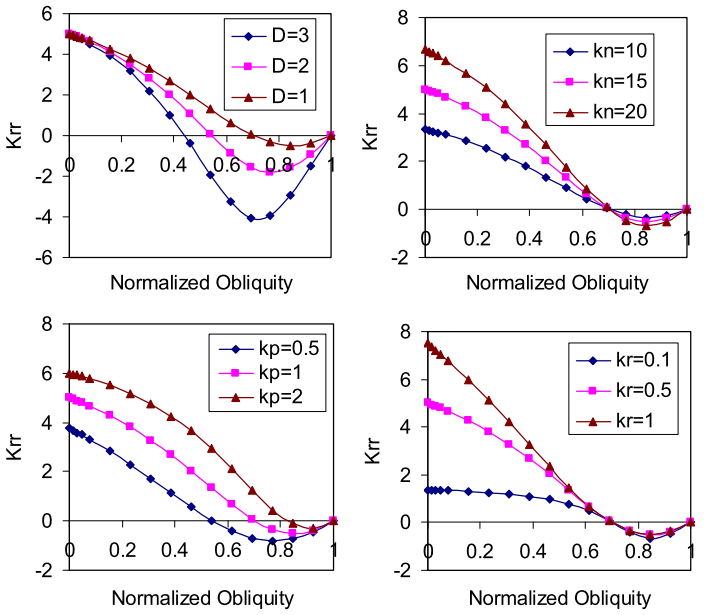

Fig. 6. Evolution of K_{rr} with obliquity for different values of the material parameters.

$$K_{rn} = k_{n0}\left(\frac{k_{rR}k_{n0}}{B_0}\frac{f_r}{f_n}\right)\left(\frac{f_n}{f_{\text{ref}}}\right)^n \tag{39}$$

$$K_{rr} = k_{n0}\left(k_{rR} - \frac{k_{rR}^2 k_{n0}}{B_0}\right)\left(\frac{f_n}{f_{\text{ref}}}\right)^n \tag{40}$$

with

$$B_0 = \frac{k_{pR}k_{n0}(\tan\phi_p - \frac{f_r}{f_n})^2}{\tan^2\phi_p} + k_{rR}k_{n0} - k_{n0}\left(\tan\phi_p - \frac{f_r}{f_n}\right)\frac{f_r}{f_n}D \tag{41}$$

where k_{rR} and k_{pR} are the elastic and plastic ratios between tangential and normal stiffness, respectively.

5.2. Failure modes

The instability conditions at the contact level can be analysed from the constitutive matrix $\overline{\overline{K}}$ shown in Eq. (36) in a contact plane. The following two modes of failure are observed regarding matrix $\overline{\overline{K}}$.

- Plastic limit condition (Mode 1)
  This mode is related to the singularity of the elasto-plastic tangential stiffness matrix. From Eqs. (37)–(41), it can be shown that when $f_r/f_n = \tan\phi_p$, the plastic modulus k_p approaches zero and $B_0 = k_{rR}k_{n0}$, which leads to the vanishing of K_{nr} and K_{rr}. Thus, the determinant of $\overline{\overline{K}}$ equals zero. In this case, the system bifurcates with the occurrence of unlimited displacement rates, which is considered as the onset of localization. The condition of $f_r/f_n = \tan\phi_p$ is the "limit locus", no shear force can exist beyond this locus.
- Divergence failure mode (Mode 2)
  As seen in Section 2, this mode is related to the loss of positiveness of the second-order work, and (depending upon the loading conditions applied) can give rise to an abrupt increase in kinetic energy. The corresponding mechanical state is reputed unstable.

The local expression of the second-order work is:

$$W_2 = \delta f_n \delta d_n + \delta f_r \delta d_r = K_{nn}(\delta d_n)^2 + (K_{nr} + K_{rn})\delta d_n \delta d_t + K_{rr}(\delta d_r)^2 \tag{42}$$

It can be shown from Eqs. (37)–(41) that the value of K_{rr} may become zero before the limit locus is reached. When $K_{rr} = 0$, the second-order work could become zero under certain combinations of incremental displacements, such as

Table 1
Model parameters for fine Hostun sand.

e_{ref}	p_{ref} (Mpa)	λ	ϕ_μ (°)	ϕ_0 (°)	m	D
1	0.01	0.2	30	30	1	1

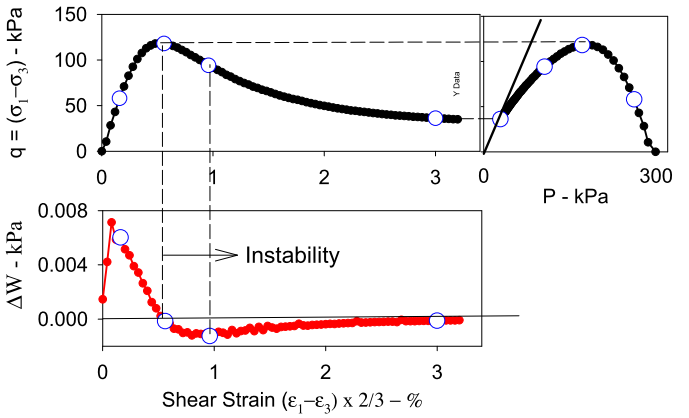

Fig. 7. Second-order work and stress–strain curves for undrained triaxial test on loose Hostun sand.

$\delta d_n = 0$. Under this condition, $K_{rr} = 0$, but the value of K_{nr} is not zero. Thus, the determinant $\overline{\overline{K}}$ may still remain positive and the rate of displacement is limited in the mode 2 failure. Note that in the case of $D = 0$ (associated flow rule), the condition of zero second-order work would occur simultaneously with the singularity of matrix $\overline{\overline{K}}$.

It is worth emphasizing that the mode 2 failure is dependent on the direction of the loading increment. For this reason, a mechanical state associated with a negative value of the second-order work is said in the sequel to be potentially instable [5,6,16]. Moreover, the failure described here is related to one contact plane, which is a sub-system of the micromechanical model. This is perfectly in line with the basic concept of the multiscale approach presented in Sections 3 and 4. Hence, the occurrence of failure is investigated on the contact plane scale in what follows.

The likelihood of $K_{rr} = 0$ is evaluated based on a set of typical parameters for Hostun sand [38,42,43], $k_{pR} = 1$, $k_{rR} = 0.5$, $D = 1$, $k_{n0} = 15$ N/mm and $\tan\phi_\mu = 0.65$. For simplicity, it is assumed that $\tan\phi_p$ is constant and independent of the material density (i.e., $\tan\phi_p = \tan\phi_\mu$). The computed values of K_{rr} is plotted in Figs. 6 against the normalized obliquity defined as $f_r/f_n \tan\phi$. Figs. 6(a, b, c, d) show the influences of the chosen values of $D = 1$–3, $k_{n0} = 10$–20 N/mm, $k_{pR} =$ 0.5–2, and $k_{rR} = 0.1$–1. For all cases, the value of K_{rr} becomes negative before the normalized obliquity reaches 1. Thus, it is clear that, for a typical range of parameters, the value of K_{rr} is likely to become zero before the obliquity reaches the plastic limit locus, and, as a consequence, the mode 2 failure is likely to prevail.

A local vanishing of the microscopic second-order work acting on the contact plane scale does not necessarily imply the vanishing of the macroscopic second-order work on the whole specimen scale. However, in some cases, the local failure along several contact planes will coalesce and result in a global instability of the overall system, which will be discussed in the following section.

5.3. Global and local behaviours

Fig. 7 presents a numerical simulation of an undrained triaxial test on loose Hostun sand with an initial confining stress $\sigma_{3c} = 300$ kPa [11]. The value of k_{t0}/k_{n0} is commonly about 0.4, corresponding to a Poisson's ratio for Hostun sand $\nu = 0.2$ and the exponent $n = 0.5$. From drained triaxial test results, we were able to derive the values of the two parameters corresponding to the position of the critical state in the e–p' plane: $\lambda = 0.2$ and $p_{ref} = 0.01$ MPa for $e_{ref} = e_{max} = 1$, and the value $m = 1$ was determined from the test results. The values of k_{p0} are assumed to be same as those of the elastic stiffness $k_{p0} = k_n$. The set of parameters for fine Hostun sand is presented in Table 1.

The second-order work in the case of axisymmetric loading can be written:

$$W_2 = \delta q \delta\varepsilon_1 + \delta\sigma_3' \delta\varepsilon_v \tag{43}$$

For undrained conditions ($\delta\varepsilon_v = 0$), the second-order work becomes reduced to $W_2 = \delta q \delta\varepsilon_1$. Since the axial strain increases continuously, $\delta\varepsilon_1$ is always positive and the second-order work can become non-positive if and only if $\delta q < 0$ (i.e., decrease in q). Therefore, a potential instability appears at the deviatoric stress peak.

In order to gain insight into the material behaviour at the interparticle level, we selected several contact planes oriented in six different directions indicated by the branch vectors, as shown in Fig. 8. The six directions are defined by the angle γ between the vector n perpendicular to the contact plane and the vertical axis.

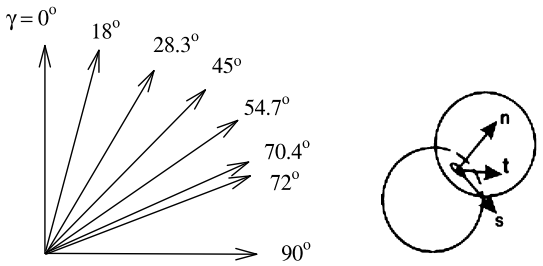

Fig. 8. Orientations of the inter-particle contact planes selected in the analysis.

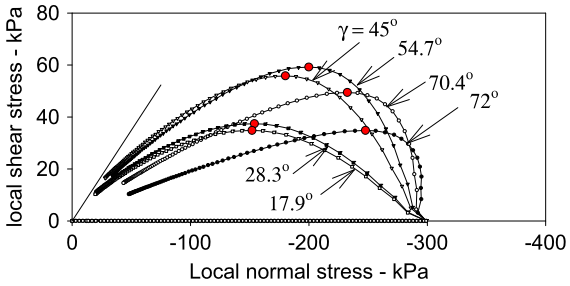

Fig. 9. Local stress paths in inter-particle contact planes.

For more direct comparison between the local and the overall stress–strain behaviour, we retained the following variables, local strain and local stress, instead of interparticle force and interparticle displacement. For this purpose, we define in each contact plane a local normal stress $\sigma^\alpha = f_n^\alpha Nl/3V$ and a local shear stress $\tau^\alpha = f_r^\alpha Nl/3V$, where l is the branch length and N/V is the total number of contacts per unit volume. The corresponding local normal strain is defined as $\varepsilon^\alpha = d_n^\alpha/l$ and the local shear strain is defined as $\gamma^\alpha = d_r^\alpha/l$.

The local stress paths in the six selected contact planes are plotted in Fig. 9. It is of interest to know whether all contact planes experience a potential instability at once. In order to answer this question, we computed the second-order work for each individual plane. Note that in an undrained test, the overall volume change is zero, but the local normal strain does not need to remain constant ($\delta\varepsilon^\alpha \neq 0$). Thus, the second-order work for the αth contact plane, expressed in terms of local stress and local strain, is given by:

$$W_2^\alpha = \delta\sigma^\alpha \delta\varepsilon^\alpha + \delta\tau^\alpha \delta\gamma^\alpha \tag{44}$$

The second-order work for the six contact planes is plotted in Fig. 10. It can be seen that only part of the contact planes experience a potential instability, and this potential instability on each plane occurs at different times, some before the global potential instability and some afterwards (see the solid circle in Fig. 10 showing the onset of global instability). For the two less-inclined contact planes at 17.9° and 28.3°, the second-order work is always positive; therefore, these two planes remain stable during the entire undrained triaxial test. For the four more-inclined contact planes oriented between 45° and 72°, the second-order work displays negative values, but does not become negative simultaneously in each plane. A potential instability occurs first in the two contact planes with inclination angles 45° and 54.7°. Then, the number of potentially instable interparticle planes continues to increase, while the assembly remains stable. After a few additional load steps, a potential instability occurs subsequently in the contact planes with inclination angles of 70.4° and 72°.

The global potential instability occurs only after several contact planes (inclined at 45°–54.7°) start to become potentially unstable. Even though several of the inter-particle planes are still stable at this time, the unstable condition of these planes is severe enough for the overall assembly to experience potential instability. This can be seen by the vanishing of the global second-order work at this point. The second-order work for the overall assembly is equal to the summation of the local second-order work for all planes:

$$\mathrm{d}^2 W = \sum_\alpha \mathrm{d}^2 w^\alpha = \frac{1}{V}\sum_\alpha \mathrm{d}f_i^\alpha \,\mathrm{d}\delta_i^\alpha = \frac{3}{N}\sum_\alpha \left(\mathrm{d}\sigma^\alpha \,\mathrm{d}\varepsilon^\alpha + \mathrm{d}\tau^\alpha \,\mathrm{d}\gamma^\alpha\right) \tag{45}$$

Thus, the global potential instability occurs at the condition of zero sum of all the local second-order works. After this point, the overall stress–strain response shows a decrease of the deviatoric stress and, progressively, more inter-particle contact planes become potentially instable.

On the other hand, the material can fail in mode 1 under specific loading conditions, when the plastic limit locus is reached. It can be noted from Eq. (41) that the singularity of a contact stiffness matrix k_{ij}^α would simultaneously cause the singularity of the overall stiffness matrix of the assembly C_{ijkl}. Therefore, the global failure (of mode 1) of the assembly will

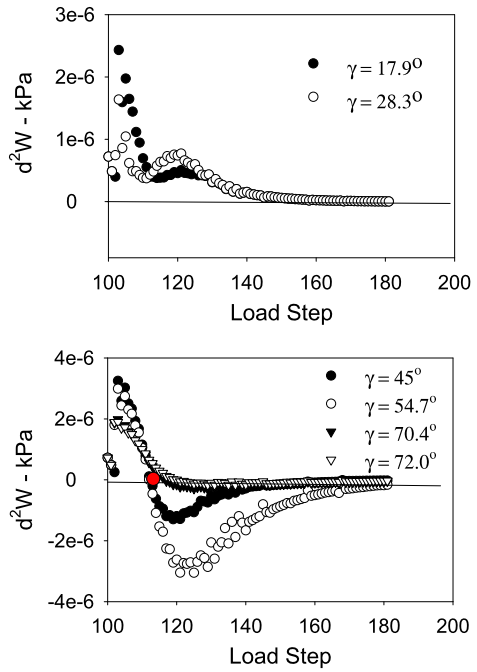

Fig. 10. Second-order work in inter-particle contact planes. The solid dot indicates the instability state of the whole assembly.

occur as soon as one local plane has failed in mode 1. This result has been confirmed by numerical simulations of drained triaxial tests [18].

6. Concluding remarks

It is well-known that failure is generally accompanied by a burst of kinetic energy. In this paper, we have shown the link between second-order work and kinetic energy, which explains the fundamental reason why the second-order work is regarded as the proper failure criterion. Indeed, when its value, at least in one loading direction, becomes negative, a necessary condition of failure is in place.

For granular materials, considered as discrete or continuous materials, depending on the scale of analysis, the second-order work is expressed (i) at the grain scale as a function of intergranular forces and displacements, and (ii) at the representative elementary volume scale as a function of the macroscopic stress and strain tensors. The link between both these expressions is demonstrated analytically and discussed in Section 3. Let it be emphasized that an inertial micro term takes into account the local avalanches, which occur at grain scale during the macroscopic plastic strain development. It shows that this analytical discrete analysis is quite detailed and complete for describing a granular assembly.

Up to now, two different approaches have been developed to take into account the discrete nature of granular media: (i) a numerical approach using discrete element methods, and (ii) a constitutive modelling approach, using micromechanical models. These two approaches have been used in this study to confirm the validity of the second-order work as a failure criterion.

The numerical simulations made by the discrete element method allowed us to examine the directional character of the macroscopic second-order work, depending on the loading direction. We found some “instability cones”, the locus of all unstable directions, which agreed with the theory. The previously established analytical link between the local discrete second-order work and the global macroscopic second-order work has been validated and discussed in a detailed manner.

The micromechanical modelling shows two different failure modes: mode 1 obtained by the plastic limit condition (singularity of the elasto-plastic matrix) and corresponding to a localized failure; mode 2 described by the second-order work criterion (loss of positive definitiveness of the elasto-plastic matrix) and corresponding to a diffuse failure.

Finally, isochoric (“undrained”) triaxial compressions were analysed by the micromechanical model, leading to a discussion on the link between locally unstable planes (defined from the model) and global instability.

Acknowledgements

The authors would like to express their sincere thanks to the French Research Network MeGe (Multiscale and multi-physics couplings in geo-environmental mechanics GDR CNRS 3176, 2008–2011) for having supported this work.

References

[1] R. Hill, A general theory of uniqueness and stability in elastic–plastic solids, J. Mech. Phys. Solids 6 (1958) 236–249.
[2] P.V. Lade, Static instability and liquefaction of loose fine sandy slopes, J. Geotech. Eng. 118 (1992) 51–71.
[3] M.R. Kuhn, S.C. Chang, Stability, bifurcation, and softening in discrete systems: a conceptual approach for granular materials, Int. J. Solids Struct. 43 (2006) 6026–6051.
[4] A. Tordesillas, M. Muthuswamy, On the modeling of confined buckling of force chains, J. Mech. Phys. Solids 57 (4) (2009) 706–727.
[5] F. Nicot, L. Sibille, F. Darve, Bifurcation in granular materials: an attempt at a unified framework, Int. J. Solids Struct. 46 (2009) 3938–3947.
[6] F. Nicot, L. Sibille, F. Darve, Failure as a bifurcation toward a dynamic regime, Int. J. Plast. 29 (2012) 136–154.
[7] F. Nicot, F. Darve, A micro-mechanical investigation of bifurcation in granular materials, Int. J. Solids Struct. 44 (2007) 6630–6652.
[8] F. Nicot, N. Hadda, F. Bourrier, L. Sibille, R. Wan, F. Darve, Inertia effects as a possible missing link between micro and macro second-order work in granular media, Int. J. Solids Struct. 49 (2012) 1252–1258.
[9] F. Nicot, F. Darve, Micro-mechanical investigation of material instability in granular assemblies, Int. J. Solids Struct. 43 (2006) 3569–3595.
[10] R.G. Wan, M. Pinheiro, P.J. Guo, Elastoplastic modelling of diffuse instability response of geomaterials, Int. J. Numer. Anal. Methods Geomech. 35 (2010) 140–160.
[11] C. Chang, P.Y. Hicher, A. Daouadji, Investigating instability in granular materials by means of a microstructural model, Eur. J. Environ. Civ. Eng. 13 (2) (2009) 167–186.
[12] L. Sibille, F. Donzé, F. Nicot, B. Chareyre, F. Darve, Bifurcation detection and catastrophic failure, Acta Geotech. 3 (1) (2008) 14–24.
[13] L. Sibille, F. Nicot, F. Donzé, F. Darve, Analysis of failure occurrence from direct simulations, Eur. J. Environ. Civ. Eng. 13 (2) (2009) 187–202.
[14] F. Darve, L. Sibille, A. Daouadji, F. Nicot, Bifurcations in granular media, macro- and micro-mechanics, C. R., Méc. 335 (2007) 496–515.
[15] A. Daouadji, H. AlGali, F. Darve, A. Zeghloul, Instability in granular materials: an experimental evidence of diffuse mode of failure for loose sands, J. Eng. Mech. 136 (5) (2010) 575–588.
[16] F. Darve, G. Servant, F. Laouafa, H.D.V. Khoa, Failure in geomaterials, continuous and discrete analyses, Comput. Methods Appl. Mech. Eng. 193 (27–29) (2004) 3057–3085.
[17] L. Sibille, F. Nicot, F. Donze, F. Darve, Material instability in granular assemblies from fundamentally different models, Int. J. Numer. Anal. Methods Geomech. 31 (2007) 457–481.
[18] C. Chang, Z. Yin, P.Y. Hicher, Micromechanical analysis for inter-particle and assembly instability of sand, J. Eng. Mech. 137 (3) (2011) 155–169.
[19] A.E.H. Love, A Treatise of Mathematical Theory of Elasticity, Cambridge University Press, Cambridge, 1927.
[20] J. Weber, Recherches concernant les contraintes intergranulaires dans les milieux pulvérulents, Bull. Liais. Ponts Chauss. (20) (1966) 1–20.
[21] J. Christofferson, M.M. Mehrabadi, S. Nemat-Nassar, A micromechanical description on granular material behaviour, J. Appl. Mech. 48 (1981) 339–344.
[22] M.M. Mehrabadi, M. Oda, S. Nemat-Nasser, On statistical description of stress and fabric in granular materials, Int. J. Numer. Anal. Methods Geomech. 6 (1982) 95–108.
[23] R. Hill, The essential structure of constitutive laws for metal composites and polycrystals, J. Mech. Phys. Solids 15 (2) (1967) 79–95.
[24] V. Šmilauer, E. Catalano, B. Chareyre, S. Dorofeenko, J. Duriez, A. Gladky, J. Kozicki, C. Modenese, L. Scholtès, L. Sibille, J. Stránský, K. Thoeni, Yade reference documentation. Yade documentation, in: V. Šmilauer (Ed.), The Yade Project, 1st ed., 2010, http://yade-dem.org/doc/.
[25] P.A. Cundall, O.D.L. Strack, A discrete numerical model for granular assemblies, Geotechnique 29 (1979) 47–65.
[26] P.A. Cundall, Distinct element models for rock and soil structure, in: E.T. Brown (Ed.), Analytical and Computational Methods in Engineering Rock Mechanics, George Allen and Unwin, London, 1987, pp. 129–163.
[27] G. Gudehus, A comparison of some constitutive laws for soils under radially symmetric loading and unloading, in: W. Wittke (Ed.), 3rd Int. Conf. Numerical Methods in Geomechanics, vol. 4, Aachen, Balkema Publisher, 1979, pp. 1309–1324.
[28] F. Darve, F. Laouafa, Instabilities in granular materials and application to landslides, Mech. Cohes.-Frict. Mater. 5 (8) (2000) 627–652.
[29] K. Wallton, The effective elastic moduli of a random packing of spheres, J. Mech. Phys. Solids 35 (1987) 213–226.
[30] C.S. Chang, Micromechanical modeling of constructive relations for granular material, in: M. Satake, J.T. Jenkins (Eds.), Micromechanics of Granular Materials, 1988, pp. 271–279.
[31] C.S. Chang, S.S. Sundaram, A. Misra, Initial moduli of particulate mass with frictional contacts, Int. J. Numer. Anal. Methods Geomech. 13 (6) (1989) 626–641.
[32] F. Emeriault, B. Cambou, Micromechanical modelling of anisotropic non-linear elasticity of granular medium, Int. J. Solids Struct. 33 (18) (1996) 2591–2607.
[33] C.L. Liao, T.C. Chan, A.S.J. Suiker, C.S. Chang, Pressure-dependent elastic moduli of granular assemblies, Int. J. Numer. Anal. Methods Geomech. 24 (2000) 265–279.
[34] P.Y. Hicher, C.S. Chang, Anisotropic non linear elastic model for particulate materials, J. Geotech. Geoenviron. Eng. 132 (8) (2006) 1052–1061.
[35] J.T. Jenkins, O.D.L. Strack, Mean-field inelastic behavior of random arrays of identical spheres, Mech. Mater. 16 (1993) 25–33.
[36] S. Nemat-Nasser, J. Zhang, Constitutive relations for cohesionless frictional granular material, Int. J. Plast. 18 (2002) 531–547.
[37] F. Nicot, F. Darve, A multi-scale approach to granular materials, Mech. Mater. 37 (2005) 980–1006.
[38] C. Chang, P.-Y. Hicher, An elastoplastic model for granular materials with microstructural consideration, Int. J. Solids Struct. 42 (14) (2005) 4258–4277.
[39] C.L. Liao, T.P. Chang, D. Young, C.S. Chang, Stress–strain relationship for granular materials bases on hypothesis of best fit, Int. J. Solids Struct. 34 (31–32) (1997) 4087–4100.
[40] R.D. Mindlin, Microstructure in linear elasticity, Arch. Ration. Mech. Anal. 16 (1969) 51–78.
[41] J. Biarez, P.Y. Hicher, Elementary Mechanics of Soil Behaviour, Balkema, The Netherlands, 1994, 208 pages.
[42] P.-Y. Hicher, Elastic properties of soils, J. Geotech. Eng. 122 (8) (1996) 641–648.
[43] P.-Y. Hicher, Experimental behavior of granular materials, in: B. Cambou (Ed.), Behavior of Granular Materials, Springer, Wien, New York, 1998, pp. 1–97.